Eur. Phys. J. A **25**, 275–282 (2005)
DOI 10.1140/epja/i2005-10107-2

THE EUROPEAN PHYSICAL JOURNAL A

Contribution of boundness and motion of nucleons to the EMC effect

B.L. Birbrair, M.G. Ryskin[a], and V.I. Ryazanov

Petersburg Nuclear Physics Institute Gatchina, St. Petersburg 188300, Russia

Received: 5 April 2005 / Revised version: 9 June 2005 /
Published online: 5 September 2005 –
Communicated by A. Schäfer

Abstract. The kinematical corrections to the structure function of the nucleon in the nucleus due to the boundness and motion of nucleons arise from the excitation of the doorway states for one-nucleon transfer reactions in the deep inelastic scattering on nuclei.

PACS. 25.30.Mr Muon scattering (including the EMC effect) – 11.10.St Bound and unstable states; Bethe-Salpeter equations – 13.60.Hb Total and inclusive cross-sections (including deep-inelastic processes)

1 Introduction

It is known for more than 20 years that the cross-section of the deep inelastic scattering (DIS) on a nuclear target is not equal to the sum of cross-sections on free nucleons [1]. This means that the interaction inside the nucleus distorts the parton distribution in a nucleon. But at first it is necessary to single out the kinematical effects arising from the boundness and motion of nucleons in nuclei because otherwise it is hardly possible to conclude what actually happens with the nucleon structure functions in nuclear matter. This is the aim of our work rather than the explanation of the EMC effect. The above kinematical effect is due to the fact that the four-momentum of the nucleon in the nucleus is not equal to that of a free nucleon. Indeed, the heavy photon (γ^*) is absorbed by a single nucleon and the deep inelastic scattering (DIS) proceeds via the following stage[1]:

$$l \;+\; A \;\to\; l' \;+\; X \;+\; (A-1)^* \;,$$

where l and l' denote the incoming and outgoing leptons, X is the final hadronic state after the γ^*-nucleon interaction and A is the target nucleus. Before absorbing the heavy photon (γ^*) the struck nucleon has a certain energy-momentum distribution in the nucleus. Besides this, the "residual" $(A-1)$ nucleus is excited.

There were a few attempts to account for the Fermi motion, boundness and the change of the effective γ-nucleon flux factor inside the nucleus [2–4] (see [5] and references therein for more details). They all were based on the seemingly obvious assumption that the energy-momentum distribution of the struck nucleon is described by the ground-state one-nucleon spectral function,

$$S_g(\mathbf{p},\varepsilon) = \left\langle A_0 \left| a^\dagger(\mathbf{p})\delta\Big(\varepsilon + H - \mathcal{E}_0(A)\Big)a(\mathbf{p})\right| A_0 \right\rangle \;, \tag{1}$$

where $|A_0\rangle$ is the ground state of the target nucleus A, $a(\mathbf{p})$ and $a^\dagger(\mathbf{p})$ are operators of the nucleon with momentum $\mathbf{p}$ (the spin and isospin variables are omitted), H is the nuclear Hamiltonian in the second quantization and $\mathcal{E}_0(A)$ is the ground-state binding energy of the nucleus A. The calculations [3] were performed by using the following semiempirical model for the quantity (1): the nucleon energy distributions were described by the experimental data on the separation energies of protons from the $(e,e'p)$ reactions [6] (the difference between the proton and neutron separation energies was neglected leading to about 10% error) and calculating the momentum distributions within the harmonic-oscillator model with the parameter $\hbar\omega_0 = (45\,A^{-1/3} - 25\,A^{-2/3})$ MeV reproducing the observed r.m.s. radii of nuclei.

Both the flux factor [4] and the correlations arising from the interaction between nucleons are disregarded in [3]. The inclusion of these effects is attempted in subsequent works. In [7] the ground-state spectral function was calculated within the Correlated Basis Function theory [8] by taking into account the two-particle NN forces only thus neglecting the multiparticle ones. But the latter is in conflict with the observed energies of deep hole states in doubly closed-shell nuclei [9]: as follows from these data

[a] e-mail: ryskin@thd.pnpi.spb.ru

[1] We will focus on the region of a not too small Bjorken $x > 0.2$ where the characteristic interaction time and distances ($\sim 1/mx$) are less than the nucleon-nucleon separation in the nucleus.

the three-particle and four-particle forces are of the same magnitude as the two-particle ones [10].

In [11] the nuclear-structure function is expressed through that of the unphysical nucleus consisting of point nucleons [12]. But to get the agreement with experiment they used unreasonably large separation energies: they put 40 MeV for ^{12}C and 45 MeV for ^{56}Fe, whereas in the neighbouring closed-shell nuclei ^{16}O and ^{40}Ca the average separation energies are 23.6 MeV and 26.5 MeV only [9].

For the above reasons the results [7] and [11] are inconclusive.

However, nobody realized in this connection that the DIS on nuclei is a rapid process, and therefore the energy-momentum distribution of the struck nucleon is described by the spectral function of the nuclear mode which is excited via a sudden perturbation rather than that of the ground state. Our work is based on the fact that the relevant mode is provided by the doorway states for the one-nucleon transfer reactions. As demonstrated in [10,13,14] the above states are eigenstates of the nucleon in the static nuclear field.

Recall that the microscopic nuclear models are based on certain approximations for the in-medium nucleon mass operator M. For instance, the nuclear shell model potential is the approximation for the mass operator at the nuclear Fermi surface, the optical model potential is dealing with the mass operator at low and intermediate energies, etc. In all the available approaches the mass operator includes all the Feynman diagrams which are irreducible in the one-particle channel, and therefore it cannot be calculated. Instead it is described by a set of phenomenological parameters.

In contrast to the above models, the nuclear static potential is the mass operator at the infinite value of the energy variable. Only the Hartree diagrams with the free space (*i.e.* vacuum) nuclear forces survive in this case, thus permitting the model-independent calculation of the static field. So the doorway states (DS) under consideration appear to be the unique nuclear object, both model-independent and described by the exactly soluble problem.

The calculation [13] showed that the r.m.s. radii of the DS density distributions are appreciably less than those of the ground-state ones: for instance, the value of $\langle r^2\rangle = A^{-1}\int \rho(r) r^2 \mathrm{d}^3 r$ is 10.88 fm^2 for the ground state of ^{40}Ca being only 8.76 fm^2 for the DS. As a result, the nucleon motion (*i.e.* the value of $\langle \mathbf{p}^2\rangle$) was underestimated in [3] by about 25% [2].

In sect. 2 we briefly describe the formalism of the DS. In sect. 3 the DIS structure functions F_2 are calculated for different nuclei and deuteron; to single out the boundness and motion effects we disregarded the possible changes of the parton distribution inside the nucleon in the nucleus. In the last section we compare the calculated ratios $2F_{2A}/AF_{2D}$ with the available experiments.

[2] For the same reason the kinematical effect was underestimated in ref. [15] as well.

2 Doorway states for one-nucleon transfer reactions

2.1 Theory

The evolution of the state arising from the one-nucleon transfer to the nuclear ground state $|A_0\rangle$ at the initial time moment $t = 0$ is described by the single-particle propagator [16],

$$\begin{aligned} S(x,x';\tau) &= -i\langle A_0|T\psi(x,\tau)\psi^\dagger(x',0)|A_0\rangle \\ &= i\theta(-\tau)\sum_j^{(A-1)} \Psi_j(x)\Psi_j^\dagger(x')e^{-iE_j\tau} \\ &\quad -i\theta(\tau)\sum_k^{(A+1)} \Psi_k(x)\Psi_k^\dagger(x')e^{-iE_k\tau}. \end{aligned} \tag{2}$$

At $\tau < 0$ it describes the evolution of the hole state,

$$\Psi_j(x) = \langle (A-1)_j|\psi(x)|A_0\rangle\ , \quad E_j = \mathcal{E}_0(A) - \mathcal{E}_j(A-1)\ , \tag{3}$$

when the nucleon is removed from the ground state A_0, whereas at $\tau > 0$ the evolution of the particle state is described,

$$\Psi_k(x) = \langle A_0|\psi(x)|(A+1)_k\rangle\ , \quad E_k = \mathcal{E}_k(A+1) - \mathcal{E}_0(A)\ , \tag{4}$$

when the nucleon is added to the ground state A_0. The quantities $\mathcal{E}_j(A-1)$, $\mathcal{E}_k(A+1)$ and $\mathcal{E}_0(A)$ are the total binding energies of the states $|(A-1)_j\rangle$ of the $(A-1)$ nucleus, the states $|(A+1)_k\rangle$ of the $(A+1)$ nucleus and the ground state $|A_0\rangle$ of the A one.

The Fourier transform of the propagator

$$\begin{aligned} G(x,x';\varepsilon) &= \int S(x,x';\tau)e^{i\varepsilon\tau}\mathrm{d}\tau = \\ &\sum_j^{(A-1)} \frac{\Psi_j(x)\Psi_j^\dagger(x')}{\varepsilon - E_j - i\delta} + \sum_k^{(A+1)} \frac{\Psi_k(x)\Psi_k^\dagger(x')}{\varepsilon - E_k + i\delta}\ , \\ &\delta \to +0\,, \end{aligned} \tag{5}$$

obeys the Dyson equation

$$\begin{aligned} \varepsilon G(x,x';\varepsilon) &= \delta(x-x') + \hat{k}_x G(x,x';\varepsilon) \\ &\quad + \int M(x,x_1;\varepsilon)G(x_1,x';\varepsilon)\mathrm{d}x_1\ , \end{aligned} \tag{6}$$

where $\hat{k}_x$ is the kinetic energy and the mass operator $M(x,x';\varepsilon)$ includes all Feynman diagrams which are irreducible in the one-particle channel.

We are interested in the very beginning of the evolution, *i.e.* the $\tau \to 0$ limit. According to the time-energy Heisenberg relation this is equivalent to the limit $\varepsilon \to \infty$. In this limit

$$G(x,x';\varepsilon) = \frac{I_0(x,x')}{\varepsilon} + \frac{I_1(x,x')}{\varepsilon^2} + \frac{I_2(x,x')}{\varepsilon^3} + \cdots\ , \tag{7}$$

where (see definition (1) of the propagator)

$$I_0(x,x') = \sum_j^{(A-1)} \Psi_j(x)\Psi_j^\dagger(x') + \sum_k^{(A+1)} \Psi_k(x)\Psi_k^\dagger(x')$$
$$= i\Big[S(x,x';+0) - S(x,x';-0)\Big], \quad (8)$$
$$I_1(x,x') = \sum_j^{(A-1)} E_j\Psi_j(x)\Psi_j^\dagger(x') + \sum_k^{(A+1)} E_k\Psi_k(x)\Psi_k^\dagger(x')$$
$$= -\Big[\dot S(x,x';+0) - \dot S(x,x';-0)\Big], \quad (9)$$
$$I_2(x,x') = \sum_j^{(A-1)} E_j^2\Psi_j(x)\Psi_j^\dagger(x') + \sum_k^{(A+1)} E_k^2\Psi_k(x)\Psi_k^\dagger(x')$$
$$= -i\Big[\ddot S(x,x';+0) - \ddot S(x,x';-0)\Big], \quad (10)$$

the quantities I_0, I_1 and I_2 thus describing the very beginning of the evolution $\left(\dot S = \frac{\partial S}{\partial \tau}, \ddot S = \frac{\partial^2 S}{\partial \tau^2}\right)$.

Now consider the mass operator $M(x,x';\varepsilon)$. It includes the energy-independent Hartree diagrams $U_{st}(x)\delta(x-x')$ (which were shown in fig. 3 of ref. [14]), the higher-order diagrams describing the nuclear correlation effects (the lowest-order diagram of such kind was shown in fig. 4a of ref. [14]) and the Fock ones (fig. 4b of ref. [14]). The correlation diagrams include the propagators of intermediate states thus behaving as ε^{-1} in the $\varepsilon \to \infty$ limit (see ref. [17] for a more stringent demonstration). The same is valid for the Fock diagrams. Indeed, the interaction between baryons proceeds via the exchange by some particles (they are quark-antiquark pairs and/or gluons in the QCD) and therefore both the momentum and the energy are transferred through the interaction. As a result, the Fock diagrams also include the intermediate-state propagators thus being of order of ε^{-1} in the $\varepsilon \to \infty$ limit. (In ref. [10] this is demonstrated for the meson-nucleon intermediate state). So the mass operator in this limit is

$$M(x,x';\varepsilon) = U_{st}(x)\delta(x-x') + \frac{\Pi(x,x')}{\varepsilon} + \cdots \quad (11)$$
$$\varepsilon \to \infty\,.$$

Introducing the static Hamiltonian

$$h_{st} = \hat k_x + U_{st}(x)\,, \quad (12)$$

let us write down the high-energy limit Dyson equation in the form

$$\varepsilon G(x,x';\varepsilon) = \delta(x-x') + h_{st}G(x,x';\varepsilon)$$
$$+ \int\left(\frac{\Pi(x,x_1)}{\varepsilon} + \cdots\right) G(x_1,x';\varepsilon)\mathrm{d}x_1\,. \quad (13)$$

Putting into (13) the asymptotics (7) and equating the coefficients at the same powers of ε^{-1}, we get

$$\sum_j^{(A-1)} \Psi_j(x)\Psi_j^\dagger(x') + \sum_k^{(A+1)} \Psi_k(x)\Psi_k^\dagger(x') = \delta(x-x'), \quad (14)$$

$$\sum_j^{(A-1)} E_j\Psi_j(x)\Psi_j^\dagger(x') + \sum_k^{(A+1)} E_k\Psi_k(x)\Psi_k^\dagger(x') =$$
$$h_{st}\delta(x-x'), \quad (15)$$

$$\sum_j^{(A-1)} E_j^2\Psi_j(x)\Psi_j^\dagger(x') + \sum_k^{(A+1)} E_k^2\Psi_k(x)\Psi_k^\dagger(x') =$$
$$h_{st}^2\delta(x-x') + \Pi(x,x'). \quad (16)$$

Equations (9), (12) and (15) may be written as

$$-\Big[\dot S(x,x';+0) - \dot S(x,x';-0)\Big] = h_{st}\delta(x-x') =$$
$$[k_x + U_{st}(x)]\,\delta(x-x')\,. \quad (17)$$

As follows from the l.h.s. of (17), the Hamiltonian h_{st} describes the very beginning of the one-nucleon transfer process the eigenstates of h_{st} thus being the doorway states for the one-nucleon transfer reactions. On the other hand, the r.h.s. of (17) shows that the Hamiltonian h_{st} describes the motion of the nucleon in the nuclear static field $U_{st}(x)$. Indeed, the latter is expressed through the free-space NN forces rather than the effective ones, thus being the nucleon field rather than the quasiparticle one. So we proved that the doorway states for the one-nucleon transfer fast reactions are the eigenstates of the nucleon in the nuclear static field.

2.2 Doorway eigenfunctions

Since the doorway states (DS) describe the motion of the nucleon in the nuclear *static* field, the corresponding eigenfunctions may be calculated in a model-independent way. Indeed, the two-particle forces are determined from the experimental data on the elastic nucleon-nucleon scattering (*i.e.* from the phase shifts analysis) [18] and the deuteron properties. The necessary information about the multiparticle forces is obtained from the observed energy spectra of the doorway states [10]. So the only additional information needed for the calculation of the static field in a given nucleus is that on the nucleon density distributions in this nucleus. In all the nuclei which are treated in the present paper these distributions are spherically symmetric thus leading to the static field with the same symmetry. Hence, the quantum-mechanical problem is the motion of a particle in a central field. This problem is solved with any desired accuracy and without any simplifications.

We have to emphasize that the doorway states are not the eigenfunctions of the total nuclear Hamiltonian thus being fragmented over the actual nuclear states owing to the correlation effects. The observed spreading width

of the DS is about 20 MeV; that is the relaxation time $\sim 0.3 \cdot 10^{-22}$ s. This is much larger than the time characteristic for DIS which is of the order of $2q_0/Q^2 \simeq 1/mx \sim 3 \cdot 10^{-24}$ s in the nucleus rest frame. So during the DIS process the DS do not have time to be distorted by the correlations thus permitting the exact account for the nucleon boundness and motion to the EMC effect.

The relevant energy-momentum distribution of nucleons for DIS is determined by the spectral function of the DS (rather than the ground-state one):

$$S_{\rm DS}(\varepsilon,\vec{p}) \;=\; S_p(\varepsilon,\vec{p}) \;+\; S_n(\varepsilon,\vec{p})\;, \qquad (18)$$

where the proton spectral function is

$$S_p(\varepsilon,\vec{p}) \;=\; \frac{1}{4\pi}\sum_{\lambda}^{(p)} \nu_\lambda f_\lambda(\vec{p})\delta(\varepsilon-\varepsilon_\lambda)\;. \qquad (19)$$

The sum in the r.h.s. runs over the proton DS, λ stands for the angular momentum j and other quantum numbers of a particle state in the central field, ν_λ is equal to $2j+1$ for the filled states and the actual number of nucleons on partly filled ones, ε_λ are the DS energies and $f_\lambda(p)$ are found by solving the Dirac equation (see refs. [10,14] for details):

$$h_{st}\psi_\lambda(\vec{r}) \;=\; \varepsilon_\lambda\psi_\lambda(\vec{r})\;. \qquad (20)$$

The function $f_\lambda(p) = u^2_\lambda(p) + w^2_\lambda(p)$, given by the sum of the upper and lower components square of the bi-spinor $\psi_\lambda(p)$ (in momentum space), is normalized by the condition

$$\int f_\lambda(p)p^2{\rm d}p \;=\; 1\;. \qquad (21)$$

The neutron spectral function obeys the same relation in which the proton DS are substituted by the neutron ones.

It is instructive to mention that the spectral functions $S_{\rm DS}(\varepsilon,\vec{p})$ is evidently Lorentz invariant obeying the following normalization:

$$\int S_{\rm DS}(\varepsilon,\vec{p}){\rm d}\varepsilon{\rm d}^3p \;=\; \int S_{\rm DS}(p){\rm d}^4p \;=\; A \qquad (22)$$

(here $p_0 = m+\varepsilon$, so ${\rm d}p_0 = {\rm d}\varepsilon$).

The calculations were performed for ^{12}C, ^{14}N, ^{27}Al, ^{40}Ca, ^{56}Fe and ^{63}Cu. The reason is as follows. As mentioned above, the necessary information for the calculations is that about the proton and neutron density distributions. The former is available throughout the whole periodic system [19], but this is not the case for the latter: the neutron densities are available only for the doubly closed-shell nuclei ^{16}O, ^{40}Ca, ^{90}Zr and ^{208}Pb [20]. That is why we confined ourselves to nuclei with a small neutron excess: the density distributions per nucleon are nearly the same for protons and neutrons in these nuclei [21].

To calculate the eigenfunctions, the Bonn-B [18] and OSBEP [22] NN-potentials were used[3]. In both cases the results are very close to each other. The difference never exceeds 0.5% for $x < 0.6$ and is less than the experimental error bars in the domain where the ratio (25) $R_{th} > 1$.

[3] For the deuteron the Bonn-B wave function was used in both cases.

3 Deep inelastic cross-section on the nuclear target

The DIS cross-section is usually written in terms of the structure function $F_2(x,Q^2)$, that is the cross-section of electron-nucleon interaction,

$$\frac{{\rm d}\sigma}{{\rm d}x{\rm d}Q^2} \simeq \frac{4\pi\alpha^2}{xQ^4}\left((1-y+\frac{y^2}{2})F_2(x,Q^2) - \frac{y^2}{2}F_L(x,Q^2)\right), \qquad (23)$$

where we neglect the nucleon mass $m_N^2 = m^2$ in comparison with the total energy square $s = (k+p)^2 \gg m^2$. Here: k, q, p are the 4-momenta of the incoming electron, heavy photon and the target nucleon, respectively. $Q^2 = -q^2$, $x = Q^2/2(p\cdot q)$ and $y = (q\cdot p)/(k\cdot p)$. $\alpha = 1/137$ is the electromagnetic coupling.

As a rule, the data are taken at rather small y, where the coefficient $y^2/2$ in front of the longitudinal part (F_L) is small. Next, the ratio $R^L = F_L/F_2 \sim 0.2$ is not large. Moreover, unlike the F_2, the function R^L does not appear to depend on the atomic number A [5].

Therefore, the ratio of the cross-sections is given usually in terms of the ratio of the structure functions F_2.

In order to compare our results with the data, where experimentalists already accounted for the difference between proton and neutron, we write the structure function of the nucleus as

$$\begin{aligned}\frac{1}{A}F_{2A}(x,Q^2) &= \frac{1}{A}\left(ZF_{2pA} + NF_{2nA}\right)\\ &= \frac{F_{2nA}(x,Q^2)+F_{2pA}(x,Q^2)}{2}\\ &\quad + \frac{N-Z}{2A}(F_{2nA}-F_{2pA})\end{aligned} \qquad (24)$$

and select the isospin $I = 0$ part of F_2 given by the first term of (24). The ratio which we will discuss reads

$$R_{\rm kin}(x,Q^2) = \frac{F_{2nA}(x,Q^2)+F_{2pA}(x,Q^2)}{F_{2D}(x,Q^2)}\;. \qquad (25)$$

The structure function of the proton in the nucleus

$$F_{2pA}(x,Q^2) \;=\; \frac{1}{Z}\sum_{\lambda}^{(p)}\nu_{p\lambda}F_{2p\lambda}(x,Q^2)\;, \qquad (26)$$

where $\nu_{p\lambda}$ is the actual number of protons on the level λ ($\nu_{p\lambda} = 2j+1$ for the completely occupied shell). Note that in the experimental data the variable x was calculated assuming the proton momentum p_N equal to the momentum of a free proton at rest, $p_N = (m_N, 0, 0, 0)$. However, to single out the precise "kinematics", one must account for the change of the nucleon structure function (parton distributions) in the medium caused by the change of the Bjorken variable $x = Q^2/2(p\cdot q)$. In other words, calculating the momentum fraction x' carried by the quark we need to use the precise four-momentum of the nucleon in the medium. That is,

$$x' = \frac{Q^2}{2(pq)} \;=\; \frac{Q^2}{2(p_0q_0 - \vec{p}\,\vec{q})} \;=\; \frac{mx}{m+\varepsilon_\lambda - \beta pt}\;, \qquad (27)$$

where $\beta = |\vec{q}|/q_0 = (1 + \frac{4m^2x^2}{Q^2})^{1/2}$ and the variable t is the cosine of the angle between $\vec{p}$ and $\vec{q}$.

Next we have to note that the structure function F_2, which at the LO reads

$$F_2 \;=\; \sum_f e_f^2(xq_f(x) + x\bar{q}_f(x)) \qquad (28)$$

(e_f is the electric charge of the quark of flavour f), contains two factors: the quark (antiquark) distribution $q(x)$ ($\bar{q}(x)$) and the kinematical factor x. The origin of this kinematical factor is as follows. The covariant quantity is not the cross-section but the discontinuity of the dimensionless interaction amplitude $\mathrm{Im}\, A \simeq s\sigma$. Going from the amplitude A to the cross-section $\sigma \propto 1/Q^2$, we obtain the factor $x_A = Q^2/2(pq)$ which corresponds to the true nucleus target and must be calculated as $x_A = AQ^2/2m_A\nu$, where m_A is the mass of the nucleus and $\nu = q_0$ is the photon energy in the nucleus rest frame. As discussed in sect. 2.2 the time of DIS on nuclei is at least an order of magnitude less than the nuclear relaxation one. This time interval is insufficient to measure the exact total mass of the target nucleus: only its part

$$m_A \;=\; \sum_\lambda^{(p)} \nu_{p\lambda}(m + \varepsilon_{p\lambda}) + \sum_\lambda^{(n)} \nu_{n\lambda}(m + \varepsilon_{n\lambda}) \qquad (29)$$

associated with the doorway states can be fixed in such conditions. For this reason we have to use the quantity m_A as the target nucleus mass. This provides both the baryon charge conservation (in a sense this is equivalent to the prescription given in [4], where the authors accounted for the relativistic flux factor and used the baryon charge conservation to normalize the spectral functions of protons and neutrons) and the validity of the energy-momentum sum rule, thus avoiding the problem mentioned in refs. [23,24]. Indeed, the total 4-momentum, that is the energy of the nucleus in its rest frame, carried by partons in the nucleus, is m_A within our prescription (as a rule, the m_A value is about 3% less than the actual ground-state mass of the nucleus[4]).

Thus, in (26) we need to calculate the function

$$F_{2p\lambda}(x,Q^2) = \frac{1}{2}\int_0^{p_\lambda} f_\lambda(p)p^2\mathrm{d}p \int_{-1}^{1} \frac{x_A}{x'} F_{2p}(x',Q^2)\mathrm{d}t$$
$$+\frac{1}{2}\int_{p_\lambda}^{\infty} f_\lambda(p)p^2\mathrm{d}p \int_{-1}^{p_\lambda/p} \frac{x_A}{x'} F_{2p}(x',Q^2)\mathrm{d}t\ . \qquad (30)$$

Here $p_\lambda = ((1-x)m + \varepsilon_\lambda)/\beta$, and $f_\lambda(p)$ was defined in sect. 2.2 [5].

Exactly the same formulae is used for the neutron in the nucleus.

For the deuteron

$$F_{2D}(x,Q^2) = \frac{1}{2}\int_0^{p_D} f_D(p)p^2\mathrm{d}p \int_{-1}^{1} \frac{x_D}{x'_D}(F_{2p}(x'_D,Q^2)$$
$$+F_{2n}(x'_D,Q^2))\mathrm{d}t$$
$$+\frac{1}{2}\int_{p_D}^{\infty} f_D(p)p^2\mathrm{d}p \int_{-1}^{p_D/p} \frac{x_D}{x'_D}\Big(F_{2p}(x'_D,Q^2)$$
$$+F_{2n}(x'_D,Q^2)\Big)\mathrm{d}t \qquad (31)$$

with

$$x'_D = \frac{mx}{m_D - \sqrt{p^2+m^2} - \beta pt}$$

and $p_D = (\beta(m_D - mx) - \sqrt{(m_D - mx)^2 + (\beta^2-1)m^2})/(\beta^2-1)$; $f_D(p)$ is just the sum of the squared monopole and quadrupole components of the deuteron wave function; m_D is the deuteron mass. Note that denominator in the expression for x'_D corresponds to the kinematics where the spectator nucleon is on-mass-shell.

The $F_{2p}(x,Q^2)$ and $F_{2n}(x,Q^2)$ free nucleon structure functions were calculated using the MRST2002 NLO parametrization [25] obtained from the global parton analysis.

4 Discussion

The results of calculations are presented in tables 1–5 and fig. 1. The predictions made using the Bonn-B and OSBEP potentials are very close to each other. So we present the results for the case of the Bonn-B potential only.

Recall that here we *assume* the parton distributions inside the nucleon in the nucleus to be the same as that for the free nucleon and evaluate the pure kinematical effect of the boundness and the motion of the nucleon in nuclear matter. Using the doorway states, which are the correct eigenfunctions to describe the fast interaction with one nucleon, we account for the full *4-momemtum* of the (target) nucleon and for the excitation of the "residual" nucleus $(A-1)$.

Thus, the difference between the calculated value of R_{kin} and the data indicates the distortion of the parton wave function of a nucleon placed in the nuclear medium.

As expected, the account of the boundness and Fermi motion of nucleons in nuclei diminishes the cross-section in the $x = 0.2$–0.63 interval. Indeed, due to the boundness (and the fact that about 24–27 MeV is spent for the excitation of the residual $(A-1)$ nucleus), the mean value of the shifted argument x' (27) is larger than the value of x on a free nucleon. On the other hand, in this domain the free-nucleon structure function F_2 falls down with x. Therefore, we get $R_{\mathrm{kin}} < 1$.

[4] For example, the "doorway" mass of ^{40}Ca is $m\,(\mathrm{doorway}) = 0.968m$ (ground state).

[5] Strictly speaking, (30) is correct for a positive p_λ only. When x is close to 1 and p_λ becomes negative, one has to keep only the last term in (30) with the integration from $-p_\lambda$ up to ∞. In this case the values of $t < 0$ and $x' < x$. So the quantity $F_{2\lambda}$ has non-zero value even at $x = 1$. Note, however, that for experimentally available x values the quantities p_λ never become negative.

Table 1. The ratio of structure functions F_2^A measured on carbon to that on deuteron. The values of Q^2 are given in GeV^2.

^{12}C		NA-037	NMC [26]	
x	Q^2	$R_{\rm exp}$	($\pm$)	$R_{\rm kin}$
.125	12.0	1.032	(.012)	0.997
.175	15.0	1.011	(.015)	0.994
.250	20.0	1.010	(.015)	0.990
.350	27.0	0.971	(.020)	0.985
.450	32.0	0.975	(.029)	0.985
.550	37.0	0.925	(.043)	0.999
.650	41.0	0.873	(.064)	1.052

Table 2. The ratio of structure functions F_2^A measured on nitrogen to that on deuteron. The values of Q^2 are given in GeV^2.

^{14}N		NA-4	BCDMS [27]	
x	Q^2	$R_{\rm exp}$	($\pm$)	$R_{\rm kin}$
.100	32.0	1.018	(.039)	0.997
.140	40.0	1.018	(.031)	0.995
.180	49.0	1.002	(.024)	0.993
.225	56.0	1.035	(.025)	0.990
.275	56.0	1.024	(.027)	0.988
.350	67.0	0.983	(.025)	0.985
.450	77.0	0.941	(.031)	0.985
.550	84.0	0.891	(.047)	0.999
.650	96.0	0.826	(.075)	1.053

Table 3. The ratio of structure functions F_2^A measured on calcium to that on deuteron. The values of Q^2 are given in GeV^2.

^{40}Ca		NA-037	NMC [28]	
x	Q^2	$R_{\rm exp}$	($\pm$)	$R_{\rm kin}$
.113	4.3	0.994	(.010)	0.998
.138	5.1	1.007	(.012)	0.996
.175	6.2	1.001	(.011)	0.994
.225	7.7	1.015	(.014)	0.990
.275	9.1	0.998	(.018)	0.986
.350	11.0	0.996	(.019)	0.981
.450	14.0	1.024	(.031)	0.978
.600	17.0	0.955	(.038)	1.005

At a large x, close to 1, the details of the angular integration (over t in (30)) become important. For a negative t, due to a Fermi motion, there is a region where $x' < x$ (see (27)). Thanks to the contribution coming from this region the value of $R_{\rm kin}$ becomes larger than 1 for $x > 0.65$–0.7.

Clearly, besides the Fermi motion there should be some dynamical effects. At a large x the growth of the ratio $R(x, Q^2)$ with x is usually attributed to short-range nucleon-nucleon correlations [31] or to multiquark bags [32] (see, for details, the reviews [5,31] and references therein). However, contrary to the conventional expectations, the theoretical value of $R_{\rm kin}$ resulting after the account of the Fermi motion in the doorway states is even *larger* than the value $R_{\rm exp}$ measured experimentally[6].

Table 4. The ratio of structure functions F_2^A measured on iron to that on deuteron. The values of Q^2 are given in GeV^2.

^{56}Fe		NA-4	BCDMS [29]	
x	Q^2	$R_{\rm exp}$	($\pm$)	$R_{\rm kin}$
.100	22.0	1.057	(.021)	0.996
.140	25.0	1.046	(.020)	0.994
.180	29.0	1.050	(.018)	0.991
.225	46.0	1.027	(.019)	0.988
.275	49.0	1.000	(.021)	0.984
.350	59.0	0.959	(.020)	0.979
.450	72.0	0.923	(.028)	0.977
.550	72.0	0.917	(.040)	0.991
.650	72.0	0.813	(.053)	1.047

Table 5. The ratio of structure functions F_2^A measured on copper to that on deuteron. The values of Q^2 are given in GeV^2.

^{63}Cu		NA-037	NMC [30]	
x	Q^2	$R_{\rm exp}$	($\pm$)	$R_{\rm kin}$
.123	11.0	1.041	(.026)	0.996
.173	16.1	1.031	(.023)	0.993
.243	19.3	1.018	(.024)	0.988
.343	25.8	0.962	(.032)	0.981
.444	36.0	0.959	(.047)	0.978
.612	46.4	0.918	(.056)	1.016

Table 6. The kinematical part $R_{\rm kin}$ of the ratio $F_2^d/[F_2^p + F_2^n]$ calculated using the Bonn-B potential.

x	$Q^2 = 5$	10	20	50	100	200 (GeV^2)
.05	$R_{\rm kin} = 1.000$	.999	.999	.999	.998	.998
.10	$R_{\rm kin} =$ .999	.999	.998	.998	.997	.997
.14	$R_{\rm kin} =$ .998	.998	.997	.997	.996	.996
.20	$R_{\rm kin} =$ .996	.996	.995	.995	.994	.994
.35	$R_{\rm kin} =$ .990	.990	.989	.989	.989	.989
.45	$R_{\rm kin} =$ .987	.987	.987	.987	.987	.987
.55	$R_{\rm kin} =$ .988	.988	.988	.989	.990	.991
.65	$R_{\rm kin} = 1.005$	1.004	1.004	1.006	1.008	1.011
.75	$R_{\rm kin} = 1.080$	1.073	1.071	1.075	1.080	1.085
.85	$R_{\rm kin} = 1.440$	1.396	1.382	1.391	1.408	1.431

[6] Since the same effect was observed both at relatively low Q^2 in SLAC data and for a larger Q^2 at CERN, this cannot be explained by the account of the mass correction.

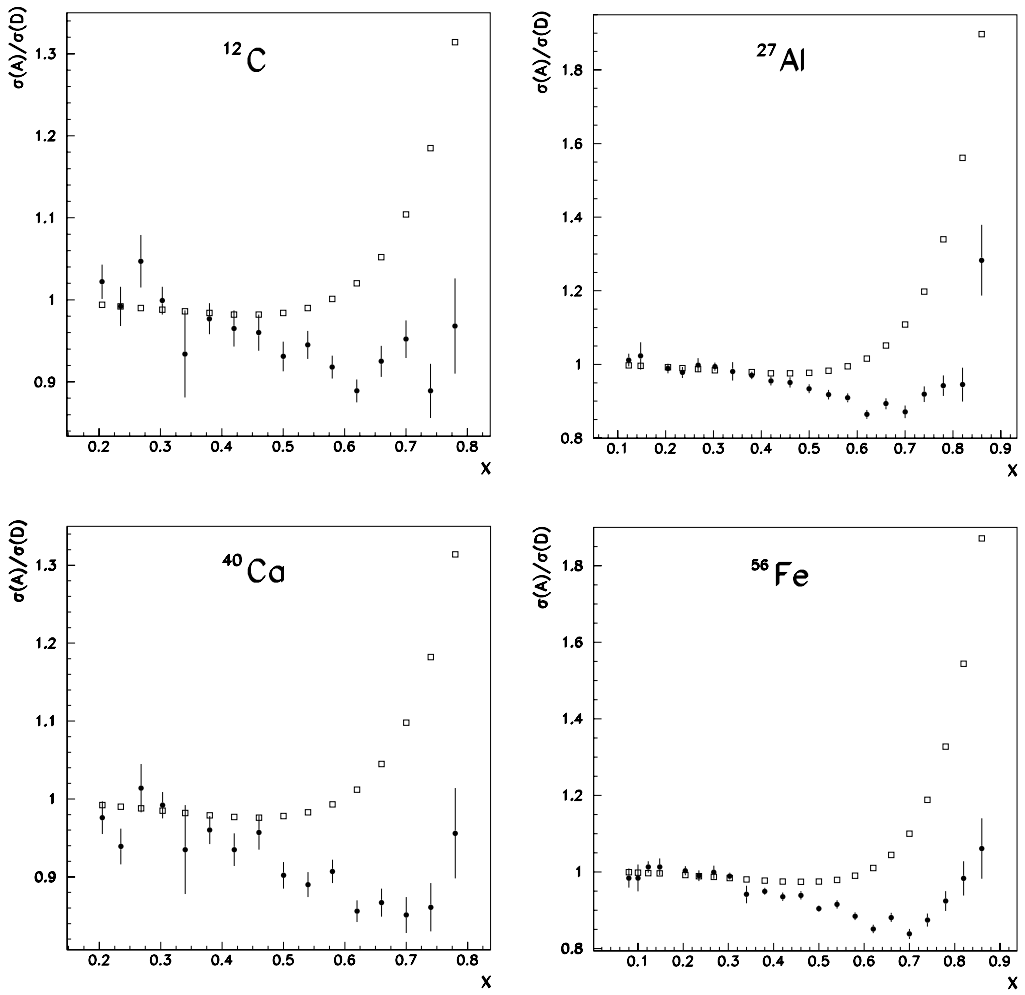

Fig. 1. The ratio of structure function F_2^A measured on the nucleus A to that on deuteron. $Q^2 = 5\,\mathrm{GeV}^2$. The data are taken from [33]. The squares are the ratio R_{kin} calculated using the Bonn-B potential.

This means that in the nuclear medium the (one-nucleon) parton distribution becomes softer, that is the probability to find a parton with $x > 0.45$ inside the in-medium nucleon is less than that in a free nucleon. In other words, in the medium the quark distribution is shifted towards a lower x, leading to a decrease of the quark density at $x > 0.45$ and to a larger quark density at a lower $x \sim 0.1$–0.2.

Next, at small $x < 0.2$ the partons from different (neighbouring) nucleons start to overlap and to interact with each other. Indeed, according to the uncertainty principle, the characteristic size of localization is $\Delta r \sim 1/mx$ and for $x < 0.2$ the value of $\Delta r > 1\,\mathrm{fm}$ becomes comparable with the nucleon-nucleon separation. At a very low x the partons screen each other and this shadowing correction results in a decreasing of $R(x, Q^2)$. Another way to describe this effect is to say that two low-x partons from two different nucleons recombine into one parton. However, the whole energy must be conserved. This leads to the antishadowing (growth of the parton density) [34] (see the reviews [5,31] for more details) just in the region ($x \sim 0.1$–0.2) of the beginning of recombination. On the other hand, this antishadowing effect is expected to reveal itself more in the gluon distributions than in the quark structure function.

Thus, it is not surprising that in the interval $0.2 < x < 0.45$ the ratio given by the pure kinematical effects, R_{kin} (25), is close (within the error bars) to that observed experimentally, R_{exp}.

Note that, at large x, the Fermi motion is not negligible, even for the deuteron. The ratio $R_{D,\mathrm{kin}} = F_{2D}/(F_{2p} + F_{2n})$ is close to unity for $x < 0.65$, but it noticeably differs from unity for $x > 0.75$, reaching values of $R_{D,\mathrm{kin}} = 1.07$ (1.42) at $x = 0.75$ (0.85), see table 6.

An analysis performed by the MRST group shows that if this effect is included, then one obtains practically the same partons, but the description of the high-x deuteron data is much improved; with χ^2 reduced by 20 for the 12 deuteron data points that are fitted at $x = 0.75$ [7].

After the present work was completed, we have read the recent paper of A. Molochkov [35] where another (but not quite different from that used here) prescription

[7] We thank R.S. Thorne and A.D. Martin for discussions and for performing a new analysis using our Fermi motion in the deuteron.

was proposed to account for the boundness and momentum distribution of nucleons. A. Molochkov had considered the ratio of the ^{4}He to deuteron structure functions. The shortness of his prescription is the assumption that both the nucleon structure function F_2 and the momentum distribution of the nucleons in the nucleus $f^N(P_A, p)$ are regular (*i.e.* have no singularities) with respect to p_0. Besides this, some terms, coming from the differentiation of the nucleus $(A-1)$ propagator and the factor $1/(p_0+\sqrt{m^2+p^2})^2$ (corresponding to the antinucleon pole) in the nucleon propagator, which are proportional to the binding (or nuclear excitation) energy, were omitted in [35]. We hope that our approach, based on the "doorway" formalism is more precise. Moreover, in terms of Molochkov's integral, our result may be obtained by closing the integration contour over p_0 in the upper half-plane (on the pole corresponding to the residue $(A-1)$ nucleus) instead of the lower one as was done in [35].

However, we are planning to compare both approaches in a forthcoming paper, using the doorway eigenfunctions to describe the distributions of nucleons in heavier nuclei.

References

1. J.J. Aubert *et al.*, Phys. Lett. B **123**, 275 (1983).
2. A. Bodek, J.L. Ritchie, Phys. Rev. D **23**, 1070 (1981); **24**, 1400 (1981).
3. S.V. Akulinichev *et al.*, Phys. Rev. Lett. **55**, 2239 (1985).
4. L. Frankfurt, M. Strikman, Phys. Lett. B **183**, 254 (1987).
5. M. Arneodo, Phys. Rep. **240**, 301 (1994).
6. S. Frullani, J. Mougey, Adv. Nucl. Phys. **14**, 1 (1984).
7. O. Benhar, V.R. Pandharipande, I. Sick, Phys. Lett., B **410**, 79 (1997); **469**, 19 (1999).
8. O. Benhar, A. Fabrocini, S. Fantoni, Nucl. Phys. A **505**, 267 (1989).
9. A.A. Vorobyov *et al.*, Yad. Fiz. **58**, 1923 (1995).
10. B.L. Birbrair, V.I. Ryazanov, Yad. Fiz. **63**, 1842 (2000).
11. A.S. Rinat, M.F. Taragin, M. Viviani, arXiv:nucl-th/0412053.
12. A.S. Rinat, M.F. Taragin, Nucl. Phys. A **598**, 349 (1996).
13. B.L. Birbrair, V.I. Ryazanov, Yad. Fiz. **64**, 471 (2001).
14. B.L. Birbrair, V.I. Ryazanov, Eur. Phys. J. A **15**, (2002) 343.
15. B.L. Birbrair *et al.*, Phys. Lett. B **166** 119 (1986).
16. A.A. Abrikosov, L.P. Gor'kov,, I.E. Dzyaloshinsky, *Methods of Quantum Field Theory in Statistical Physics* (Prentice-Hall, Englewood Cliffs, 1963).
17. A.B. Migdal, *Theory of Finite Fermi Systems and Applications to Atomic Nuclei* (Nauka, Moscow, 1983).
18. R. Machleidt, K. Holinde, Ch. Elster, Phys. Rep. **149**, (1987) 1.
19. H. de Vries *et al.*, At. Data Nucl. Data Tables **36**, (1987) 495.
20. G.D. Alkhazov *et al.*, Nucl. Phys. A **381**, 430 (1982).
21. G.D. Alkhazov, private communication.
22. L. Jäde, H.V. von Geramb, Phys. Rev. C **57**, 496 (1998).
23. V. Barone *et al.*, Z. Phys. C **58**, 541 (1993).
24. Z. Batiz, F. Gross, Phys. Rev. D **61**, 114023 (2000).
25. A.D. Martin, R.G. Roberts, W.J. Stirling, R.S. Thorne, Eur. Phys. J. C **28**, (2003) 455.
26. M. Arneodo *et al.*, Nucl. Phys. B **441**, 12 (1995).
27. G. Bari *et al.*, Phys. Lett. B **163**, 282 (1985).
28. P. Amaudruz *et al.*, Nucl. Phys. B **441**, 3 (1995).
29. A.C. Benvenuti *et al.*, Phys. Lett. B **189**, 483 (1987).
30. J. Ashman *et al.*, Zeit. Phys. C **57**, 211 (1993).
31. L.L. Frankfurt, M.I. Strikman, Phys. Rep. **160**, 235 (1988).
32. R.L. Jaffe Phys. Rev. Lett. **50**, 228 (1983); C.E. Carlson, T.J. Havens, Phys. Rev. Lett. **51**, 261 (1983); S. Date, A. Nakamura, Prog. Theor. Phys. **69**, 565 (1983); H. Faissner, B.B. Kim, Phys. Lett. B **130**, 321 (1983); H.J. Pirner, J.P. Vary, Phys. Rev. Lett. **46**, 1376 (1981); Nucl. Phys. A **358**, 413 (1981).
33. R.G. Arnold *et al.*, Phys. Rev. Lett. **52**, 727 (1984).
34. N.N. Nikolaev, V.I. Zakharov, Yad. Fiz. **21**, 434 (1975); Sov. J. Nucl. Phys. **21**, 227 (1975); Phys. Lett. B **55**, 397 (1975); Z. Phys. C **49**, 607 (1991).
35. A. Molochkov, arXiv:nucl-th/0407077